GigaScience, 2026, **15**, giag097, 1–13
https://doi.org/10.1093/gigascience/giag097
Published: 22 October 2026
Research

GONet: a molecular interaction-guided graph learning framework for multi-omics cancer classification

Yiyang Chen [1,2], **Yunning Lu** [2,3], **Da Qi** [2], **Yong Bai** [4,*], **Guixue Hou** [2,*], **Siqi Liu** [1,2,*]

[1]College of Life Sciences, University of Chinese Academy of Sciences, No. 1 Yanqihu East Rd, Huairou District, Beijing, 100049, China
[2]Department of Proteomics, BGI-Genomics, No. 9 Yunhua Road, Yantian District, Shenzhen, Guangdong, 518083, China
[3]School of Biology and Biological Engineering, South China University of Technology, Waihuan Dong Rd, Panyu District, Guangzhou, Guangdong, 510006, China
[4]BGI Research, 146 Beishan Road, Yantian District, Shenzhen, Guangdong, 518083, China
*Correspondence address. Siqi Liu, College of Life Sciences, University of Chinese Academy of Sciences, No. 1 Yanqihu East Rd, Huairou District, Beijing, 100049, China. E-mail: siqiliu@genomics.cn; Guixue Hou, Department of Proteomics, BGI-Genomics, No. 9 Yunhua Road, Yantian District, Shenzhen, Guangdong, 518083, China. E-mail: houguixue@bgi.com; Yong Bai, BGI Research, 146 Beishan Road, Yantian District, Shenzhen, Guangdong, 518083, China. E-mail: Yong.bai@hotmail.com

Abstract

Background **Integrating multi-omics profiles with molecular interaction networks enables biologically informed representation learning by combining molecular measurements with prior biological knowledge. Although graph neural networks (GNNs) are well suited for modeling molecular interaction networks, existing multi-omics methods often rely on shallow representation learning or incomplete fusion strategies, which fail to fully capture complementary information and complex dependencies across heterogeneous omics layers, resulting in suboptimal performance and limited generalizability in cancer classification tasks.**

Results **Here, we propose GONet, a hierarchical GNN framework that integrates omics expression profiles, including mRNA, miRNA, and protein data, with molecular interaction networks, where nodes represent omics features and edges represent molecular interactions. GONet learns global omics representations via an autoencoder, captures local structural dependencies using Deep Graph Infomax (DGI), and enhances omics-specific representations through an attention mechanism. A gated fusion module presentations through an attention mechanism. A further enables adaptive integration of heterogeneous features, improving cancer subtype and stage classification. GONet was systematically evaluated on 13 publicly available benchmark datasets used in prior studies, covering 10 cancer types, ensuring fair comparison across methods. Across mRNA and miRNA datasets, GONet achieved an average AUROC of 0.9262, outperforming representative GNN- and non-GNN-based methods by 13.77 and 6.35%, respectively. On an independent CPTAC cohort spanning 7 cancer types, it improved performance by 25.22 and 13.91%, respectively. Incorporating proteomics further improved cancer stage classification by 5.56%, demonstrating complementary predictive value. Ablation studies confirmed the effectiveness of the DGI-based module.**

Conclusions **Overall, GONet provides a unified framework for biologically informed multi-omics graph representation learning and cancer classification.**

Keywords multi-omics data integration, graph neural network, cancer classification, molecular interaction network

Introduction

Cancer remains one of the leading causes of morbidity and mortality worldwide [1], driven by highly complex and heterogeneous molecular mechanisms. Elucidating these mechanisms is essential for understanding cancer initiation and progression, as well as for improving clinical diagnosis, treatment, and prevention [2, 3]. The advent of high-throughput omics technologies has enabled systematic characterization of cancer across multiple molecular layers [4, 5]. Genomics reveals the landscape of genetic alterations underlying cancer development [4, 6], while transcriptomics and proteomics provide gene expression patterns, including gene expression dynamics, post-translational modifications, and molecular interactions [4, 7, 8]. In essence, cancer initiation and development are cumulative results of genetic mutations [9]; therefore, the pronounced heterogeneity of cancers is likely associated with the interactions across networks involving genome, transcriptome, and proteome [4, 10]. Although single-omics data provide rich experimental evidences and bioinformatic insights at the molecular level, from the perspective of the central dogma [11], interactions across different molecular levels during the transmission of genetic information also influence biological phenotypes [12, 13]. Consequently, integrating multi-omics information is essential for a comprehensive characterization of cancer biology

Received: 28 May 2026. **Revised:** 31 August 2026. **Accepted:** 16 October 2026
© The Author(s) 2026. Published by Oxford University Press on behalf of GigaScience. This is an Open Access article distributed under the terms of the Creative Commons Attribution License (https://creativecommons.org/licenses/by/4.0/), which permits unrestricted reuse, distribution, and reproduction in any medium, provided the original work is properly cited.

[5, 14, 15]. With continuous accumulation of large-scale resources, such as The Cancer Genome Atlas (TCGA) [3], and the Clinical Proteomic Tumor Analysis Consortium (CPTAC) [2], researchers have increasingly focused on multi-omics integration studies.

Benefiting from strong capabilities in nonlinear modeling and representation learning, deep learning has become a major methodology for multi-omics integration in cancer analysis [16–19]. Early deep learning approaches that primarily rely on non-graph neural network (GNN) architectures, such as autoencoders (AEs), multilayer perceptrons (MLPs), and attention-based models, transform different omics profiles into unified representations and alleviate problems of high dimensionality and noise. For example, MOCAT is an AE-based framework that integrates mRNA, miRNA, and DNA methylation data across multiple diseases, including Alzheimer's disease and several cancer types, achieving improved classification performance in disease diagnosis, subtype, and stage prediction [20]. Attention-based models have been introduced to enhance multi-omics representation learning by dynamically weighting contributions from different omics features. Methods such as HTML and CLCLSA combine attention mechanisms with contrastive learning strategies and achieve well-improved performance in multi-cancer classification tasks [21, 22]. GNNs, another important class of deep learning models, are designed to capture relational dependencies in graph-structured data through message passing between nodes [23–25]. Early GNN-based multi-omics approaches are primarily constructed using sample-level similarity graphs for classification tasks, in which nodes represent individual samples and edges encode pairwise relationships derived from omics features. For instance, MOGONET employs graph convolutional networks (GCNs) [26] on sample similarity graphs constructed from mRNA, miRNA, and DNA methylation data for prediction of cancer subtypes/stages [27]. MOGCN constructs sample similarity graphs from CNV, mRNA, and RPPA data in TCGA breast cancer and was applied to subtype classification [28]. However, those approaches, either traditional non-GNN or sample-similarity-based GNN models, focus on learning global representations at the sample level from the gene expression matrices to integrate omics data. As a result, they cannot utilize the interaction information and are limited in capturing complex nonlinear dependencies across omics features, thereby leaving substantial room for improvement in representation learning for disease and cancer subtype prediction.

Cancer is not solely driven by single-gene aberrations but is regulated by complex molecular interaction networks. If interaction graphs are integrated into GNN-based multi-omics integration frameworks, with nodes representing gene features and edges characterizing the feature interactions, such a design is expected to enable GNNs to learn biologically local representations from molecular interaction topology and improve disease prediction [10, 16, 29]. Recently, SynOmics has extended GCN-based [26] architectures to intra- and inter-omic interaction graphs for cancer prognosis prediction [30], while Li et al. proposed a hybrid model to improve prediction performance for breast cancer subtype classification [31], in which MLPs encode global omics profiles and GCN or GAT [32] models molecular interaction networks. Nevertheless, there remains large room for improvement in current GNN-based models. First, feature extraction is insufficient across multiple levels. MLP-based encoders tend to compress high-dimensional omics data toward task-specific representations, potentially losing informative variations. Standard message-passing in GNNs is largely confined to local neighborhoods, and may therefore have limited ability to capture broader dependencies. In addition, most current methods assume homogeneous node representations, whereas they ignore intrinsic heterogeneity across omics types such as mRNA and proteins. Therefore, a novel feature extractor is required to be capable of representing both omics characteristics and interaction patterns. Second, representation fusion remains insufficiently coordinated. Since simple concatenation may lead to unstable hierarchical representations and weak discrimination power in downstream tasks, a new fusion mechanism that can resolve conflicts and inconsistencies among multiple representations is highly desirable. Third, with the growing proteomic evidence for cancer classification, a promising avenue is to introduce proteomics and the corresponding interaction networks into GNN-based models to enhance discriminative capacity [33–36].

In this study, the GONet is proposed, a novel multi-level GNN framework for cancer classification by integration of multi-omics profiles, mRNAs, miRNAs, and proteins, with interaction networks. GONet employs autoencoders to capture global representations, and applies Deep Graph Infomax (DGI) [37] to model local representations from molecular interaction networks. Considering the heterogeneous contribution across omics, GONet introduces an attention mechanism to generate omics representations that highlight differential regulation of gene expression. Furthermore, a gated fusion module is designed in GONet to dynamically reconcile global, local, and omics-specific representations, thereby alleviating potential conflicts and improving integration consistency. Results from benchmark tests and case studies suggest that GONet can improve predictive performance across several cancer datasets.

Results

GONet: a hierarchical graph neural network for multi-omics and molecular interaction integration

GONet is a modular, end-to-end framework that synergistically integrates matrix-based multi-omics data (e.g., transcriptomics and proteomics profiles) with graph-structured biomolecular interaction networks to derive biologically meaningful, low-dimensional representations for downstream classification tasks, including cancer staging and subtyping. Accordingly, the framework comprises 2 major parts: (1) dual-input: preprocessed multi-omics matrices and a curated interaction graph upon transcriptomes and proteomics; (2) model architecture: multi-level feature extraction followed by adaptive fusion; and downstream prediction classification. A schematic overview of framework is presented in Fig. 1.

In the dual-input part, multi-omics matrices, including mRNA, miRNA, and proteomics profiles, are preprocessed into a unified matrix $X \in R^{n \times d}$, where n and d represent the number of samples and features, respectively. For each sample, the personalized molecular interaction graph $G = (V, E, H)$is constructed based on the curated interactions from public databases, in which V as nodes represents molecules, E as edges denotes interactions, and H stands for sample-specific molecular quantities (see the "Methods" section).

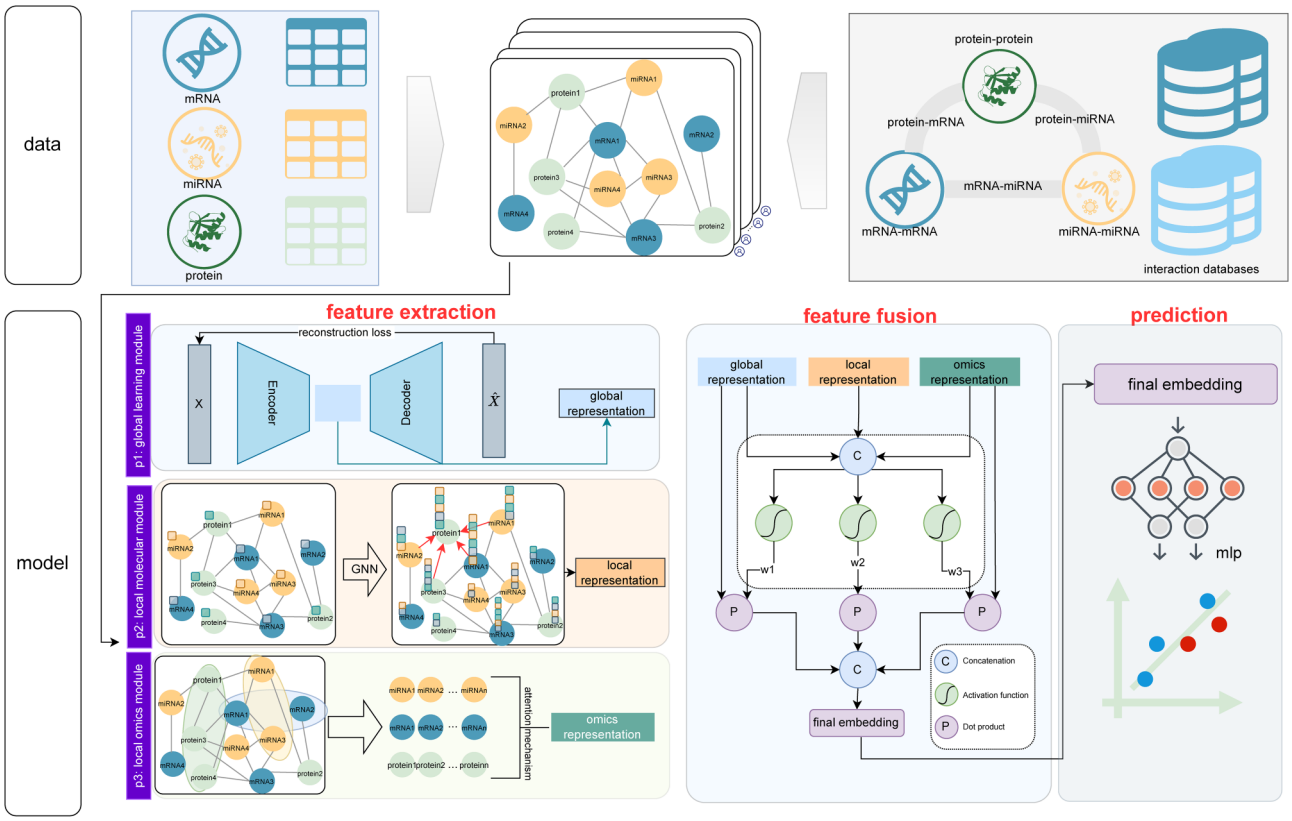


Figure 1 *Overview of the GONet framework*. GONet integrates multi-omics profiles (mRNA, miRNA, protein) with biomolecular interaction networks for cancer classification. *Data collection and graph construction*. Multi-omics datasets and curated molecular interaction networks are used to construct sample-specific molecular interaction graphs. *Model architecture*. Multi-omics matrices serve as inputs to the global learning module (AE-based), while the sample-specific molecular interaction graphs are processed by the local learning module (DGI-based). In parallel, the local omics module captures inter-omics dependencies using attention mechanism. The resulting representations are fused via feature fusion module (GFM-based) and passed to a prediction module for the downstream classification tasks.

In the model architecture part, 3 core modules are employed, feature extraction, feature fusion, and prediction. In feature extraction modules: 3 synergistic sub-modules are designed to generate complementary data representations. (A) Global sample learning: regarding the widespread application of autoencoders for dimensionality reduction in multi-omics data integration and addressing the limitation of MLP-based compression in capturing information-rich global representations, AE is applied to compress the input matrix X into a low-dimensional representation H_{global}, while the decoder reconstructs the input $\hat{X}$ by minimizing mean squared error (MSE) loss. (B) Local molecular learning: considering global representations overlook local patterns in molecular interaction networks, and that conventional GCN and GAT models suffer from over-smoothing and limited discriminative capacity, DGI is applied to maximize node-graph mutual information via the contrastive loss, generating local representations H_{local} from the molecular interaction graph G. (C) Local omics learning: addressing the lack of omics-specific information, a self-attention mechanism (SAM) [38] at omics-level adaptively weights inter-omics dependencies by learnable coefficients into H_{omics}. In feature fusion modules, an adaptive gated fusion mechanism (GFM) [39] aligns the complementary representations (H_{global}, H_{local}, and H_{omics}) from the 3 sub-modules. The GFM adaptively weights and combines the 3 representations to generate a unified representation, H_{final}, allowing the model to adjust the relative contributions of the individual modules. In prediction modules, H_{final} is passed through to a fully connected classifier, which outputs class probabilities for cancer subtype or stage prediction (Fig. 1).

Performance evaluation of GONet modules compared with previous GNN-based methods

GNN-based methods have been applied to cancer type and stage prediction using multi-omics data in recent 5 years, including approaches with or without explicit modeling of interaction information, such as MOGONET [27], MOGCN [28], SynOmics [30], and Li's method [31], MGDMCL [40], and MOGANet [41]. As shown in Fig. 2A, MOGONET and MOGCN exhibit inconsistent performance across datasets, often performing best on their original benchmark datasets. In contrast, SynOmics and Li's method demonstrate relatively more stable cross-dataset performance, suggesting that interaction information may be beneficial for effective cancer classification. However, SynOmics primarily considered the contribution of molecular interactions while underutilizing sample-level information, whereas Li's method integrates both local molecular interactions and global sample-level representations, yielding robust and generalizable multi-omics integration. Despite these advances, their representation learning and feature fusion strategies still leave room for further improvement.

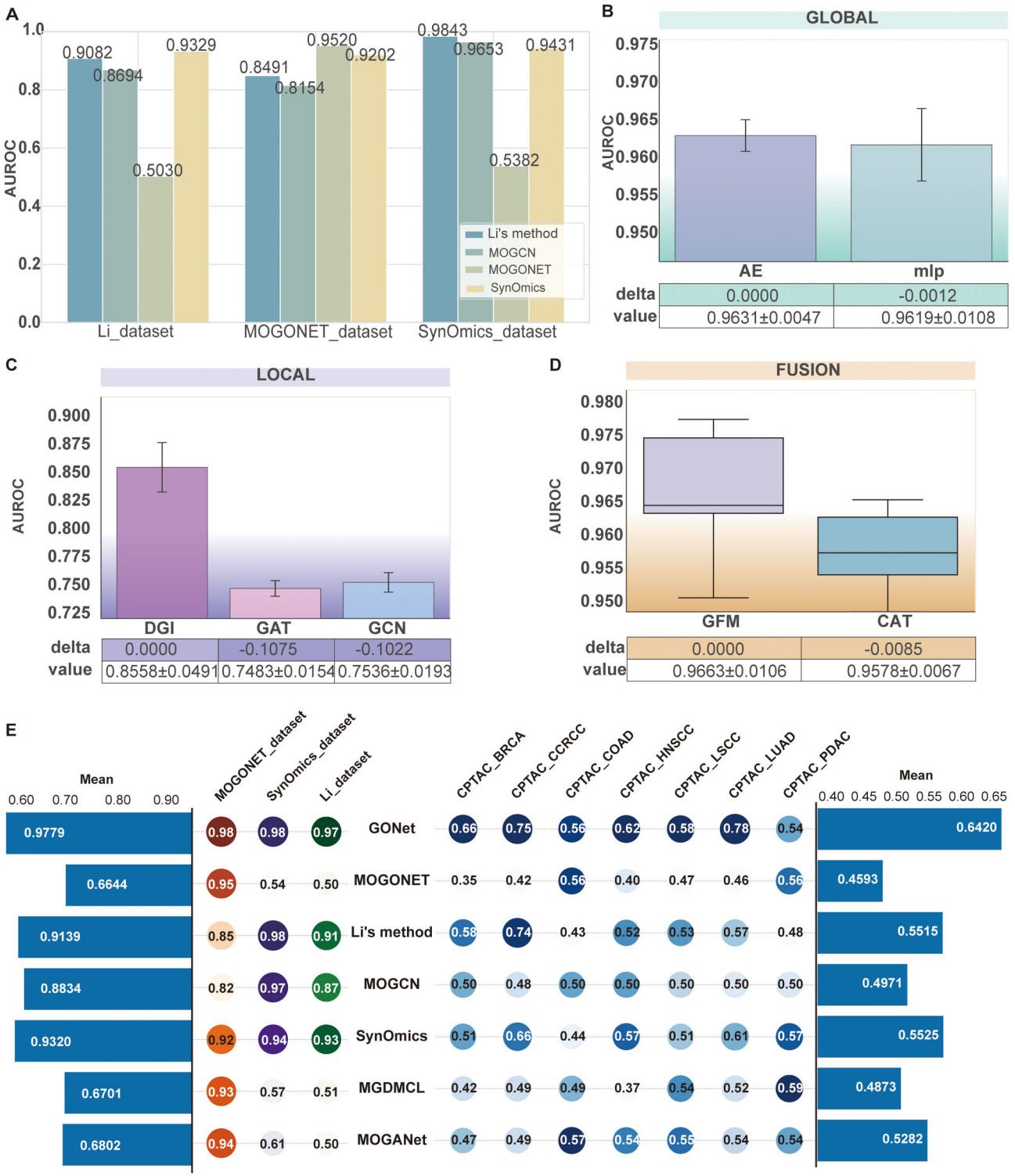


Figure 2 Module-level comparison and performance evaluation of GONet against existing GNN-based models. (A) Comparative predictive performance of representative GNN-based methods across multiple public multi-omics cancer datasets. (B–D) Module-specific evaluation of key architectural components in GONet on the BRCA subtype classification task using paired mRNA and miRNA data. (B) *Global learning module.* Performance comparison of AE in GONet with an MLP baseline. (C) *Local learning module.* Performance comparison of DGI with GCN and GAT baselines. (D) *Feature fusion module.* Comparison between the adaptive GFM used in GONet and CAT. (E) Generalization performance of GONet compared with representative GNN-based methods on original benchmark datasets (left) and CPTAC datasets (right).

To further analyze the contribution of each component, we compare GONet with Li et al.'s framework, which employs MLP-based global learning, GCN/GAT-based local learning, and concatenation-based fusion. In contrast, GONet adopts AE-based global encoding, DGI-based local learning, SAM-based omics modeling, and GFM-based fusion. Using the BRCA dataset from Li et al. (Li_dataset), all modules were evaluated independently under a unified classifier. For global learning, AE and MLP achieve comparable performance (AUROC: 0.9631±0.0047 vs. 0.9619±0.0108; Fig. 2B). For local learning, DGI significantly outperforms GCN and GAT (0.8558±0.0491 vs. 0.7536±0.0193 and 0.7483±0.0154; Fig. 2C). The SA-based omics module achieves an AUROC of 0.8077±0.039. For feature fusion, GFM slightly improves over concatenation (0.9663±0.0106 vs. 0.9578±0.0067; Fig. 2D). To further evaluate the contribution of each architectural component to entire GONet, ablation analyses were adopted on the CPTAC datasets, like removal of AE, replacement of DGI, removal of omics representation, and replacement of gated fusion. The ablation results endorsed the conclusions drawn from Fig. 2A–D, with DGI playing a role of major contributor. Detailed ablation results are provided in Supplementary Fig. S1A–D and Supplementary Tables S3 and S4. Overall, each module of GONet positively contributes to subtype classification, especially in local learning.

Performance of the full GONet framework was further evaluated for cancer subtype and stage classification in comparison with representative GNN-based methods on their original datasets using mRNA and miRNA data. As summarized in Fig. 2E, GONet was evaluated for cancer classification across the datasets used for the development of these GNN-based methods. On Li's dataset, GONet achieved an AUROC of 0.9663, representing a 6.39% improvement over Li's method (0.9082). On the MOGONET datasets, GONet yielded an AUROC of 0.9824, higher than those of MOGONET (0.9520), MGDMCL (0.9329), and MOGANet (0.9386), respectively. GONet also obtained an AUROC of 0.9849 on the SynOmics dataset, compared with 0.9431 for SynOmics. Together, these results demonstrate the improved prediction of cancer classification performance by GONet.

Next question is whether the prediction performance of GONet and the other GNN-based methods is comparable on the same omics datasets. CPTAC dataset was used for such evaluation, using mRNA and miRNA data across 7 cancer types (BRCA, CCRCC, COAD, HNSCC, LUAD, LSCC, and PDAC). As shown in Fig. 2E and Table S4, GONet consistently yielded higher prediction performance than other GNN-based methods for cancer stage classification across the CPTAC datasets, with an average AUROC of 0.6420, corresponding to 16.41% relative improvement over Li's method, 39.78% over MOGONET, 29.15% over MOGCN, 16.20% over SynOmics, 21.54% over MOGANet (0.5282), and 31.75% over MGDMCL (0.4873) ($P < 0.05$). Although performance gains are consistent, absolute AUROC values remain moderate, suggesting that dataset size and omics quality remain key limiting factors for multi-omics cancer prediction.

Proteomics contributes to GONet for cancer classification

Unlike mRNA and miRNA data, which primarily capture transcriptional information, proteomics data directly reflects the functional state of gene expression [33, 35, 42]. Besides, large-scale resources, such as BioGRID [43] and STRING [44], accumulate extensive protein–protein interaction (PPI) information, providing inherent support for GNN-based modeling. These characteristics motivate the evaluation of proteomics as an alternative omics modality within the GONet for cancer classification prediction.

To systematically assess the applicability of GONet to proteomics data, a modality substitution experiment was conducted, where transcriptomic inputs (miRNA and mRNA) were replaced with proteomics data together with corresponding PPI networks across 7 CPTAC cancer types.

As presented in Fig. 3A, GONet well accommodated the proteomics data, achieving performance comparable to transcriptomics-based models (average AUROC: 0.6360 vs. 0.6420). At the individual cancer-type level, the proteomics-based predictions achieved slightly higher AUROC values than transcriptomics-based predictions in 5 of 7 cancer types (BRCA, CCRCC, LUAD, HNSCC, and PDAC), whereas modestly lower performance was observed in COAD and LSCC. Overall, these results suggest that the proteomics data is a viable modality for GNN-based cancer stage prediction with GONet, at least in the CPTAC cohort.

An arising question concerns the relative contribution of individual omics to cancer stage prediction in GONet. As summarized in Fig. 3B, proteomics alone yielded higher predictive performance among the 3 single-omics inputs, with an average AUROC of 0.6360, compared to 0.6038 for mRNA and 0.5721 for miRNA. At the individual dataset, proteomics-based predictions outperformed those derived from either mRNA or miRNA alone in 5 of the 7 CPTAC cancer types. These results suggest that proteomics provides stronger discriminative information for cancer stage classification than mRNA or miRNA alone within the GONet framework.

Finally, we evaluated whether the integration of 3 omics data could further improve cancer stage prediction in CPTAC. As shown in Fig. 3B, the mean AUROC for tri-omics integration of miRNA, mRNA, and proteomics in GONet was 0.6777, which is obviously higher than that derived by proteomics alone (0.6360; $P < 0.05$) or transcriptomics (miRNA-mRNA:0.6420; $P < 0.05$). These results demonstrate that multi-omics integration provides complementary information, with proteomics contributing essential functional-level signals that enhance cancer stage prediction.

Performance comparison of GONet and non-GNN methods for cancer classification

A wide range of non-GNN-based multi-omics integration methods have been applied to cancer type and stage classification, including several conventional methods, such as RF [45], SVM [46], LR [47], AE, MLP, and recently published approaches, such as HTML [22], CLCLSA [21], and MOAEAM [48]. Given the strong performance of GONet compared with existing GNN-based methods, a systematic evaluation was conducted from 3 perspectives: (i) comparison with existing non-GNN methods on their original datasets and on CPTAC, (ii) evaluation under proteomics integration, and (iii) global statistical comparison across all datasets and methods.

A total of 13 datasets were recruited, including those previously studied by HTML (COAD, ESCA, GBMLGG, SARC, STAD, STES, THCA, UCEC), CLCLSA (LGG, KIPAN), MOGONET, SynOmics, and Li et al. (Table S1). All datasets contained the mRNA and miRNA profiles with cancer stage or subtype labels. Fourteen approaches,

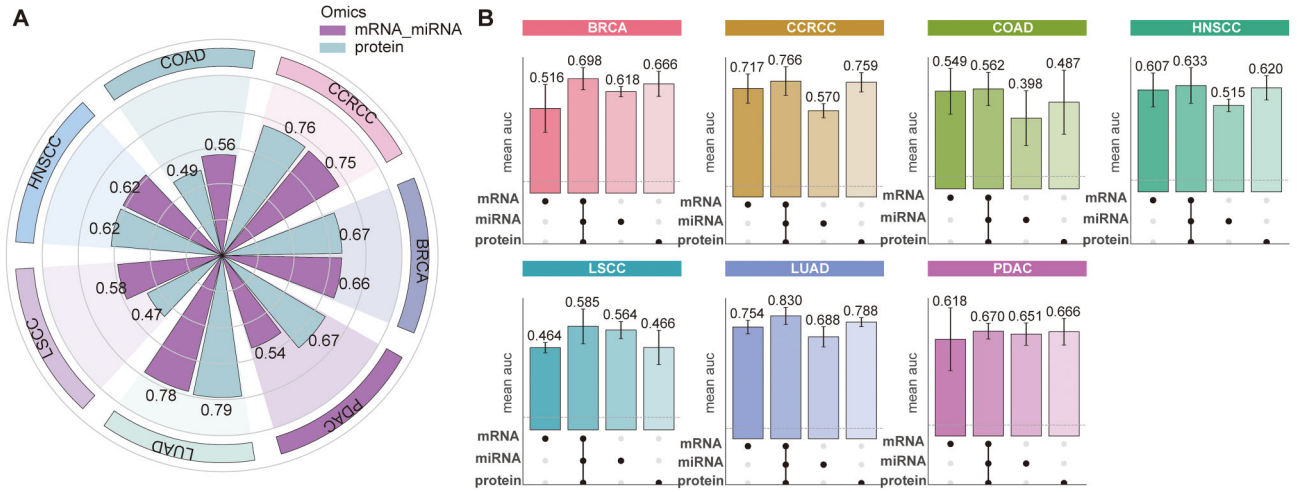


Figure 3 Evaluation of proteomics integration in GONet. (A) Comparison of transcriptomics-based (mRNA-miRNA) and proteomics-based inputs for cancer stage classification across CPTAC cohort. (B) Performance of single- and tri-omics integration (mRNA, miRNA, protein) for cancer stage classification across CPTAC datasets.

including GNN- and non-GNN-based methods, were applied onto each dataset, with results summarized in Supplementary Data (Table S1). The performance can be categorized into 3 circumstances, (1) due to unclear reason, all approaches achieved relatively poor performance on the 2 datasets HTML_GBMLGG and HTML_STAD, with AUROC ranging from 0.6297 to 0.7272 (Fig. 4A); (2) most approaches obtained near-saturated predictions on 3 datasets HTML_ESCA, HTML_STES, and HTML_KIPAN, with AUROC values exceeding 0.99 (Fig. 4B); and (3) the different approaches exhibited variable prediction performance on the remaining 8 datasets (Fig. 4C). GONet consistently showed higher prediction performance than the comparison methods, with an average AUROC of 0.9495 versus 0.8687 for the non-GNN methods. Notably, the GNN-based comparison methods showed lower prediction performance on the same datasets, with an average AUROC of 0.7465. These results strengthen our argument that improvements in representation learning and interaction modeling are critical for GNN-based multi-omics methods.

All the non-GNN methods were applied to the CPTAC datasets for assessment of cancer stage classification. As shown in Fig. 4D, these methods achieve AUROC values ranging from 0.5080 to 0.6226, all significantly lower than GONet (0.6420; $P < 0.05$). Although overall performance remains moderate across all methods, likely due to limited sample size and task difficulty, GONet consistently achieves the best performance among both GNN and non-GNN approaches.

Giving the importance of proteomics, a question is raised if non-GNN-based approaches can effectively utilize tri-omics integration (mRNA, miRNA, and proteomics) on CPTAC. As shown in Fig. 4E, non-GNN-based approaches exhibited lower predictive performance, with average AUROC values spanning 0.4780–0.6012 ($P < 0.05$). Moreover, proteomics integration led to inconsistent gains across methods and across the 7 cancer types (Fig. 4F).

Finally, a Friedman test across 27 experimental scenarios was conducted to statistically evaluate the advantages of GONet. As shown in Supplementary Fig. S5, GONet ranked first, and the null hypothesis of equal performance was rejected ($P < 0.001$), indicating that GONet achieves statistically differences in the evaluation scenarios.

Discussion

GNNs have recently emerged as a powerful approach for multi-omics data integration by incorporating molecular interaction networks, as exemplified by Li et al. and the SynOmics framework [30, 31]. However, as shown in Fig. 2A, systematic comparison of the current GNN-based approaches reveals that integration of interactions does not consistently yield improve performance, suggesting that effectiveness depends not only on the introduction of interaction information, but also on how efficiently they are leveraged. In complex cancer omics networks, conventional GCN and GAT models inherently behave as low-pass filters [49, 50], aggregating local neighborhoods information, and readily suffering from over-smoothing during propagation processes, resulting in indistinguishable node representations and reduced discriminability [50, 51]. To avoid the drawback, GONet innovatively incorporates DGI, which extracts more discriminative node representations from molecular interaction networks by maximizing mutual information between node-level representations and graph-level representations [37]. From an information-theoretic perspective, mutual information maximization captures global context and higher-order dependencies, and has been shown to improve embedding quality for downstream tasks [52, 53]. Furthermore, DGI's contrastive learning framework distinguishes real node-graph pairs from corrupted ones, encouraging robustness to noise and improving representation quality [54, 55]. Module comparison experiments confirm that the DGI markedly improves the standard GCN or GAT, yielding superior classification performance (Fig. 2C). The improvement is consistent with prior reports in biological network representation learning, in which DGI enhances representation quality and downstream task performance in molecular-disease association networks [56], PPI networks [57], and single-cell transcriptome-derived gene regulatory networks [58].

Proteins represent functional executors of biological processes, whereas transcripts primarily reflect upstream regulatory activity [59]. Accordingly, proteomics provides complementary functional and interaction-level signals, yet remains underutilized in existing approaches. Some studies integrated only protein expres-

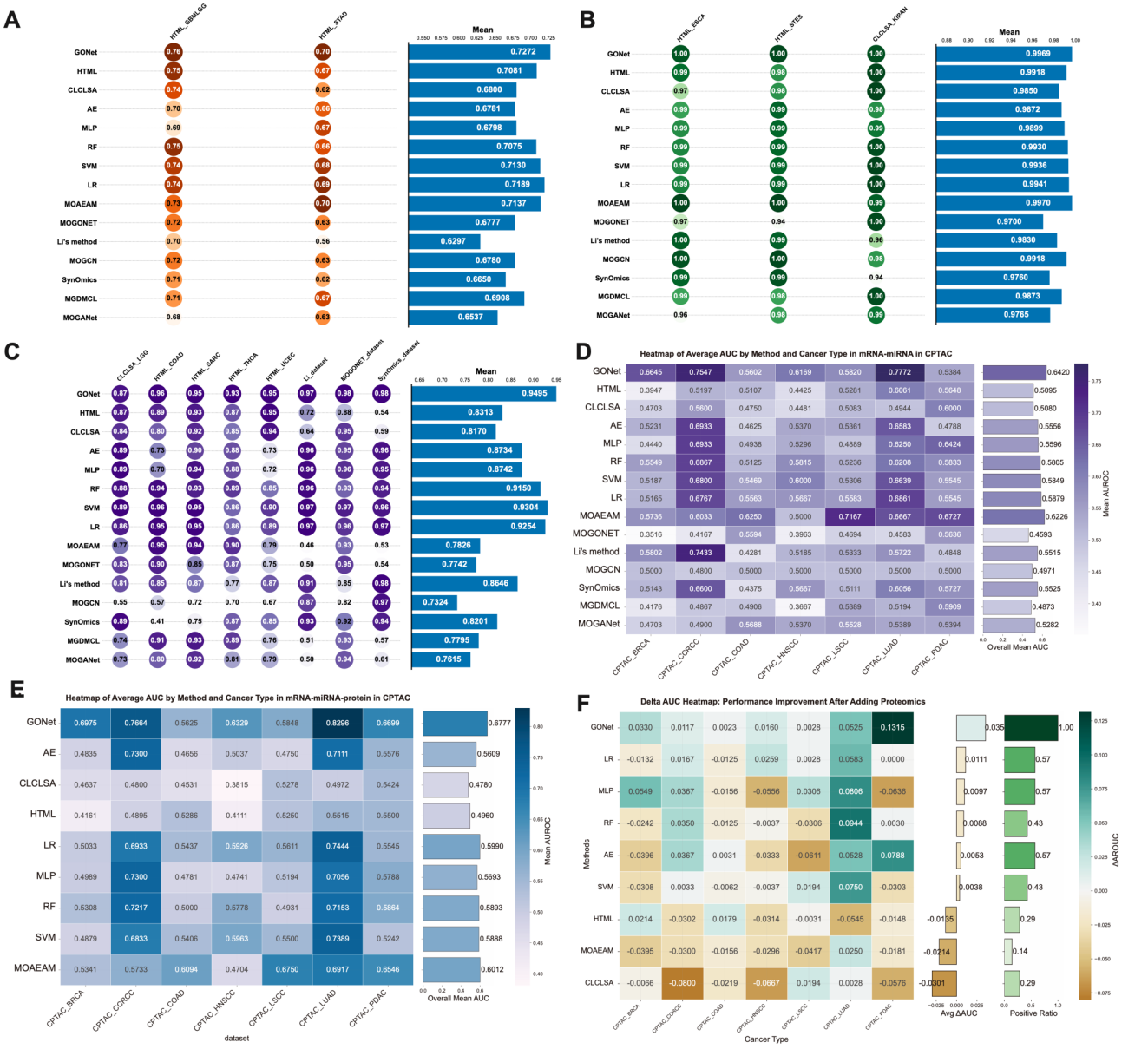


Figure 4 Systematic benchmarking of GONet performance across multi-omics cancer classification tasks. (A–C) Performance comparison for bi-omics integration (mRNA-miRNA) between GONet and 14 competing methods across 13 datasets collected from previous studies grouped by task difficulty. (D) Heatmap depicting AUROC values for bi-omics integration (mRNA-miRNA) between GONet and the 14 competing methods across 7 CPTAC cancers. (E) Heatmap showing AUROC values for tri-omics integration (mRNA, miRNA, and proteomics) between GONet and the 8 non-GNN methods across 7 CPTAC cancers. (F) Heatmap illustrating the absolute AUROC improvements (ΔAUROC) for each method after integrating proteomics data.

sion data (MOGCN with RPPA profiles [28]), while others included protein interaction networks without protein abundance, leaving synergistic modeling unexplored [31]. In this study, we simultaneously integrated protein abundance and associated interaction networks from the CPTAC cohort. Proteomes alone exhibited predictive power comparable to mRNA and miRNA, while integration with transcriptomic data further improves performance (Figs 3A, B and 4C). Ablation analysis shows that neither abundance-only nor interaction-only signals yield strong performance (AUROC = 0.6039 and 0.5587), whereas their combination yields a substantial gain (AUROC = 0.6777; Fig. S7). These results indicate that predictive improvements arise from the synergistic integration of proteomic abundance and interaction structure. Notably, although incorporation of proteome into GONet improves performance, the gain magnitude remains moderate. GONet still leaves substantial room for further improvement, primarily in 2 directions: more advanced model architectures, such as large language model-based approaches [60, 61], and larger cohort sizes to enhance deep learning capacity and better capture mRNA and protein characteristics [62].

Beyond predictive performance, exploring the relationships between GONet-based disease classification and molecular features may provide additional insights into the biological relevance of the predictions. As pointed out by Sundararajan et al., Integrated Gradients (IG) can be used to quantify the contribution of individual input features to model predictions and facilitate the identi-

fication of biologically relevant signals [63]. Further development of such interpretability analyses may provide additional biological insights into GONet-based disease classification.

In summary, a modular GNN-based framework for integration of omics data with molecular interactions, GONet, was proposed and examined its capacity in cancer types and stages classification. GONet adopts a hierarchical representation learning strategy, AE-based global encoding, DGI-based local interaction modeling, attention-based modality weighting, and gated multi-level fusion. Extensive evaluations across multiple cancer cohorts and omics settings demonstrate that GONet achieves consistently robust performance compared with both GNN- and non-GNN-based methods. Particularly, GONet enables systematic joint modeling of proteomic abundance and interaction topology, with stable performance gains when proteomics data are involved. Overall, GONet has established a multi-omics integration framework that potentially provides a methodological foundation for disease classification.

Methods

Data preprocessing

The benchmark datasets followed the original formats in previous literatures, whereas the CPTAC data were processed using the procedures described by Wang et al. and Ji et al. [27, 65]. Specifically, data preprocessing procedure followed a step-wise strategy in each random train-test split, removal of features with more than 20% missing values, imputation of remaining missing values using k-nearest neighbors (KNN), min–max normalization, and ANOVA-based feature selection were performed on the training set. And then processing procedure and selected features were applied to the corresponding independent test sets.

Molecular interaction networks

Comprehensive molecular interaction networks in this study were curated by aggregation of public interaction repositories, including PPIs derived from BioGRID [43], STRING [44], and IID [66]; mRNA-related regulatory interactions sourced from RISE [67], NPInter [68], and RNAInter [69]; and miRNA-related regulatory interactions retrieved from miRNet [70]. All interaction data were limited to human interactions, and nodes and edges involved in such interactions were further filtered to remove incomplete or erroneous records (Table S3). Molecular identifiers were standardized using UniProt IDs for proteins, HGNC symbols for mRNAs, and miRDB IDs for miRNAs.

Graph construction based on multi-omics interactions

For each patient sample s, a personalized molecular interaction graph G_s was constructed by integrating multi-omics profiles with curated interaction networks and defined as

$$G_s = (V_s, E_s, H_s),$$

where V_s represents nodes with molecular entities (mRNAs, miRNAs, and proteins) detected in sample s, with v_i and v_j correspond to 2 nodes of V_s. E_s denotes edges derived from the curated interaction networks for sample s. Each edge $e_{ij} \in E_s$ between molecules v_i and v_j is defined as

$$e_{ij} = \begin{cases} 1, & \text{if an interaction exists between } v_i \text{ and } v_j \\ 0, & \text{otherwise} \end{cases}$$

H_s corresponds to the normalized expression values of the respective molecular entities in sample s.

Construction of GONet

Global sample learning module

The AE used for global sample learning comprises an encoder and decoder.

Encoder processing. Let the original multi-omics feature matrix $X \in R^{n\times m}$ serve as input, where n represents the number of samples and m denotes the total number of molecular entities. A low dimensional global representation, $H_{\text{global}} \in R^{n\times d_g} (d_g \ll m)$, is compressed by encoder functioned $f_{enc}(\cdot)$:

$$H_{\text{global}} = f_{\text{enc}}(X),$$

where the f_{enc} consists of fully connected layers followed by LeakyReLU activations to capture non-linear patterns.

Decoder processing. The reconstructed representation $\hat{X}$ is generated from H_{global} by decoder functioned $f_{\text{dec}}(\cdot)$ to ensure that the compressed H_{global} retains the essential information of X. The reconstruction process is formulated as

$$\hat{X} = f_{\text{dec}}\left(H_{\text{global}}\right),$$

where $\hat{X} \in R^{n\times m}$ represents the approximation of original matrix X. The decoder maintains a symmetric architecture with the encoder.

Reconstruction loss. The AE parameters are optimized by minimizing reconstruction loss L_{rec} between X and $\hat{X}$, defined as

$$L_{\text{rec}} = \| X - \hat{X} \|_2^2,$$

where $\| \quad \|_2^2$ is defined as the MSE.

Local molecular learning module

DGI model for local molecular learning is applied to learn high-quality local representations at 2 hierarchical scales: the node-level (individual molecules) and the graph-level (the entire molecular interaction network).

Node-level representation. For each sample s, node-level representations $H_{\text{node}} \in R^{|V_s|\times d_l}$ are learned via graph convolutional encoder GCN$(\cdot)$ that aggregates information from neighboring molecules in the sample-specific molecular interaction network G_s:

$$H_{\text{node}} = \text{GCN}(G_s),$$

where $|V_s|$ represents the number of molecule nodes in sample s, and d_l denotes the dimensionality of node representation. Each row $h_v \in H_{\text{node}}$ corresponds to a d_l-dimensional embedding of molecule v.

Graph-level representation. The graph-level representation $H_{\text{local}} \in R^{2d_l}$ is obtained by aggregating H_{node} with a dual-pooling strategy (mean and max pooling) to capture the global topology of the molecular network:

$$H_{\text{local}} = \left[\frac{1}{|V_s|}\sum_{v\in V_s} vh_v\right] \oplus \left[\max_{v\in V_s} h_v\right],$$

where $\oplus$ denotes vector concatenations, and the left and right part indicate pooling strategies to generate $2d_l$-dimensional vector for sample s.

Maximization of mutual information. To ensure that node-level representations encode global topology information, a discriminator D is introduced to maximize the mutual information between H_{node} and H_{local}, which distinguishes between real node-graph pairs (h_v, H_{local}) from the true interaction graph G_s, and corrupted pairs $(\tilde{h}_v, H_{\text{local}})$, as described below:

$$L_{\text{DGI}} = -\frac{1}{|V_s|}\sum_{v\in V_s}\left[\log D(h_v,\ H_{\text{local}}) + \log\left(1 - D\left(\widetilde{h_v}, H_{\text{local}}\right)\right)\right],$$

where $\tilde{h}_v$ represents the corrupted node representation obtained from a corrupted graph with randomly shuffle nodes.

Local omics learning module

The local omics learning module aggregates node-level representations into omics-specific representations and integrates information from different omics through an adaptive attention mechanism.

Omics-specific representation aggregation. To reduce noise and capture omics-specific signatures, omics-specific representations H_m for each omics modality m are generated by averaging the node-level representations of its constituent molecules V_m:

$$H_m = \frac{1}{|V_m|}\sum_{v\in V_m} h_v,$$

where V_m represents the set of nodes belonging to modality m. The representations of all omics modalities are then stacked as

$$H_{\text{stack}} = \begin{bmatrix} H_1 \\ H_2 \\ \vdots \\ H_{|M|} \end{bmatrix}, \qquad H_{\text{stack}} \in R^{|M|\times d_l},$$

where $|M|$ is the number of omics.

Self-attention mechanism. To adaptively weight the contributions of different omics modalities, the attention weights A are computed as follows:

$$A = \text{softmax}\left(\frac{\sigma\left(H_{\text{stack}}W_Q\right)\left(H_{\text{stack}}W_k\right)^{\top}}{\sqrt{d_k}}\right),$$

where W_Q and W_K are learnable weight matrices and d_k is the attention dimension. The fused omics-level representation H_{omics} is obtained by weighting H_{stack} with A:

$$H_{\text{omics}} = A\left(H_{\text{stack}}W_V\right).$$

Contrastive loss. To optimize the omics module and ensure that the learned representations H_{omics} are discriminative, a supervised contrastive loss L_{sup} is minimized to encourage sample with same label y to have similar embeddings:

$$L_{\text{sup}} = \text{SupConLoss}\left(H_{\text{omics}}, y; \tau\right),$$

where τ represents the temperature hyperparameter controlling the scale of the loss.

Feature fusion module

The feature fusion module integrates global, local, and omics representations through representation alignment followed by adaptive fusion to synthesize multi-level information.

Representation alignment. Given the different feature spaces and dimensions of H_{global} H_{local} and H_{omics}, the 3 representations are projected into aligned representations Z_{mod} with a common dimension d_f by a fully connected layer followed by a LeakyReLU activation:

$$Z_{\text{mod}} = \text{LeakyReLU}\left(W_{\text{mod}}H_{\text{mod}} + b_{\text{mod}}\right),$$
$$\text{mod} \in \{\text{global, local, omics}\},$$

where W_{mod} and b_{mod} are learnable parameters.

Representation fusion. An adaptive gated mechanism $f_{\text{Gate}}(\cdot)$ is employed to learn relative importance weights α_{mod} of each representation:

$$\alpha_{\text{mod}} = \left[\alpha_{\text{global}}, \alpha_{\text{local}}, \alpha_{\text{omics}}\right] = f_{\text{Gate}}\left(\left[Z_{\text{global}} \oplus Z_{\text{local}} \oplus Z_{\text{omics}}\right]\right),$$
$$\sum_{\text{mod}} \alpha_{\text{mod}} = 1,$$

where oplus denotes concatenation, and the gating function is implemented as a softmax operation to normalize the importance weights across the 3 modules. The final fused representation H_{final} is defined as the convex combination of the Z_{mod}:

$$H_{\text{final}} = \sum_{\text{mod}} \alpha_{\text{mod}} Z_{\text{mod}},\ H_{\text{final}} \in R^{n\times d_f}.$$

Prediction module

The prediction module performs cancer stage or subtype classification based on H_{final}, and the prediction performance is assessed using focal loss [71].

Classification prediction. The fused representation H_{final} is fed into a fully connected layer with learnable parameters W_c and b_c, followed by a softmax function to predict cancer stages or subtypes. The predicted probability vector p is computed as

$$p = \text{softmax}\left(W_c H_{\text{final}} + b_c\right).$$

Focal loss. Focal loss is used as the classification loss L_{cls}, which measures discrepancy between the predicted probability p and the true class $y \in \{1, \ldots, C\}$:

$$L_{\text{cls}} = -\alpha\left(1 - p_y\right)^{\gamma}\log\left(p_y\right),$$

where p_y represents the predicted probability for true label y, and α and γ are hyperparameter controlling class weighting and focusing strength, respectively.

Total loss function

The GONet framework is trained by minimizing a joint multi-objective loss function:

$$L_{\text{total}} = \lambda_{\text{rec}}L_{\text{rec}} + \lambda_{\text{DGI}}L_{\text{DGI}} + \lambda_{\text{sup}}L_{\text{sup}} + \lambda_{\text{cls}}L_{\text{cls}} + \lambda_{\text{reg}}L_{\text{reg}},$$

where L_{reg} is a regularization item to prevent overfitting, and trade-off hyperparameters $\{\lambda_{\text{rec}}, \lambda_{\text{DGI}}, \lambda_{\text{contra}}, \lambda_{\text{cls}}, \text{and } \lambda_{\text{reg}}\}$ control the relative contribution of each loss items.

Data splitting and model training

Each dataset was partitioned into a training set and an independent test set at an 8:2 ratio using stratified random splitting. For GONet, hyperparameters were optimized strictly in the 80% training set using 5-fold cross-validation. Based on the optimal hyperparameters determined via cross-validation, the final model was retrained on the entire 80% training set and subsequently evaluated on the held-out 20% independent test set. To assess the stability of GONet, the entire procedure was repeated 5 times using

different random seeds, and the final performance metrics were reported as the average across these 5 iterations. All comparison methods, regardless of GNN or non-GNN, were evaluated using the same train-test splits to ensure a fair and consistent benchmarking comparison (Supplementary Fig. S3). All experiments were performed on a Linux system equipped with an NVIDIA A100 GPU (80 GB VRAM). The GONet was implemented in Python 3.8, using PyTorch 2.0 with CUDA 11.8, and PyTorch Geometric (PyG) 2.4.0.

Hyperparameter optimization

The hyperparameters of GONet were optimized on the training set using Optuna [72], a framework based on Bayesian optimization principles. Specifically, the optimization was conducted within a predefined search space through many independent trials. In each trial, Optuna proposed a candidate hyperparameter configuration based on the results of previous trials, which was then evaluated using 5-fold cross-validation. The mean AUROC across the 5 folds was used as the performance metric to guide selection of the next candidate configuration of hyperparameters. After completing the optimization process, the hyperparameters configuration yielding the highest mean AUROC was selected as the final configuration for GONet (see Tables S5 and S6).

Additional files

Supplementary Figure S1. Module ablation analyses of GONet for cancer stage classification. To systematically quantify the contribution of each architectural component in GONet, module-wise ablation analyses were conducted on the cancer stage classification task using paired mRNA, miRNA, and proteomics data from 7 cancer types in the CPTAC cohort. (A) *Ablation of the global sample module:* Performance of the full GONet model was compared with a variant without the AE-based global sample learning (noAE). (B) *Ablation of local molecular module*: DGI was replaced with graph convolutional network (GCN) and graph attention network (GAT), while keeping other GONet components unchanged. (C) *Ablation of omics module*: The full GONet model was compared with a variant lacking the self-attention-based omics modeling (noOmics). (D) *Ablation of feature fusion strategy*: The adaptive gated fusion mechanism in GONet was replaced with naive feature concatenation (CAT) for integrating representations across different modules. These module-wise ablation experiments collectively quantify the individual contribution of each component and validate the overall architectural design of GONet.

Supplementary Figure S2. Interpretability analysis of GONet predictions using Integrated Gradients (IG) in an independent Fu-iCCA cohort. (A) Receiver operating characteristic curve demonstrating the subtype classification performance of GONet in the independent Fu-iCCA cohort. GONet achieved robust classification performance with an AUROC of 0.98. (B–C) Distribution of Integrated Gradients (IG) scores for the top 100 features identified from the global and local modules, stratified by molecular modality (transcriptomic and proteomic features). The results demonstrate that highly ranked predictive features were derived from both mRNA and protein modalities. (D) Sankey diagram illustrating the functional associations of the top-ranked mRNA and protein features identified by GONet. The diagram depicts the relationships among molecular features, enriched biological functions, and corresponding Fu-iCCA molecular subtypes, highlighting the biological processes and signaling pathways associated with the identified predictive features. (E) Box plots showing the subtype-specific distribution patterns of the prioritized molecular features. The consistent differential expression patterns across Fu-iCCA subtypes further support the biological relevance of the features identified by GONet.

Supplementary Figure S3. Illustration of GONet hyperparameters and training strategy. Schematic diagram depicts the key hyperparameters and training procedures employed in GONet for multi-omics cancer classification tasks. (See the “Methods” section for full optimization and training details).

Supplementary Figure S4. Illustration of data preprocessing.

Supplementary Figure S5. Average ranks of all methods across multiple benchmarking scenarios, with lower ranks indicating superior overall performance.

Supplementary Figure S6. Performance gains from proteomics integration in GONet across single- and bi-omics baselines. The incremental impact of proteomics integration was assessed by measuring the change in AUROC (ΔAUROC) when proteomics data were added to baseline models. Analyses were conducted using paired data from 7 cancer types in the CPTAC datasets. (A) Single-omics mRNA baseline: ΔAUROC observed after adding proteomics. (B) Single-omics miRNA baseline: ΔAUROC observed after introducing proteomics. (C) Bi-omics (mRNA-miRNA) baseline: ΔAUROC observed after integrating proteomics. Box plots display distributions of ΔAUROC values, with mean values annotated. These analyses highlight the quantitative benefit of proteomics integration for improving multi-omics cancer classification in GONet.

Table S1. Characteristics of public multi-omics datasets used for model training and evaluation.

Table S2. Overview of curated molecular interaction networks used for graph construction.

Table S3. Ablation analysis of individual GONet modules for cancer classification performance.

Table S4. Quantitative summary of module-wise ablation analyses of GONet across 7 CPTAC cancer cohorts for cancer stage classification.

Table S5. Detailed hyperparameter space for the GONet model.

Table S6. Detailed hyperparameter configurations for the GONet model.

Table S7. The IG scores of global module and local module within the GONet.

Availability of source code and requirements

Project name: GONet

Project home page: https://github.com/EayonYang/GONet.git

License: Apache-2.0 license

Operating system(s): Ubuntu 22.04

Programming language: Python 3.8 or higher

Other requirements: PyTorch 2.1 or higher, Pytorch Geometric 2.4 or higher, and other dependencies specified in the project repository

RRID: SCR_028640

List of abbreviations

AE: AutoEncoder; AUROC: Area Under the Receiver Operating Characteristic curve; CPTAC: Clinical Proteomic Tumor Analysis Consortium; DGI: Deep Graph Infomax; GAT: graph attention network; GCN: graph convolutional network; GFM: gated fusion mechanism; GNN: graph neural network; IG: integrated gradients; MLP: multi-layer perceptron; MSE: mean squared error; PPI: protein–protein interaction; RF: Random Forest; SAM: self-attention mechanism; SVM: support vector machine; TCGA: The Cancer Genome Atlas.

Acknowledgments

Thanks to the support of the High-performance Computing Platform of YaZhou Bay Science and Technology City Advanced Computing Center (YZBSTCACC).

Funding

The work was supported by the National Key Research and Development Program of China (grant number 2023YFC3402900).

Data availability

All datasets used in this study are publicly available from their respective original sources, including CLCLSA, HTML, MOGONET, SynOmics, and Li's dataset [21, 22, 27, 30, 31]. The CPTAC datasets were obtained from the LinkOmicsKB database [64]. Detailed information on the data sources is provided in Supplementary Table S1.

Competing interests

Some authors are affiliated with BGI, the sponsor of GigaScience. All editorial handling and peer review of this manuscript were conducted independently by the journal's editorial team in accordance with the journal's standard editorial policies and procedures to ensure transparency, objectivity, and impartiality. The authors have no additional competing interests to declare.

References

1. Bray F, Laversanne M, Sung H, *et al.* Global cancer statistics 2022: GLOBOCAN estimates of incidence and mortality worldwide for 36 cancers in 185 countries. *CA A Cancer J Clinicians*. 2024;**74**:229–263. https://doi.org/10.3322/caac.21834.
2. Li Y, Dou Y, Da Veiga Leprevost F, *et al.* Proteogenomic data and resources for pan-cancer analysis. *Cancer Cell*. 2023;**41**:1397–1406. https://doi.org/10.1016/j.ccell.2023.06.009.
3. Aaltonen LA, Abascal F, Abeshouse A, *et al.* Pan-cancer analysis of whole genomes. *Nature*. 2020;**578**:82–93. https://doi.org/10.1038/s41586-020-1969-6.
4. Manzoni C, Kia DA, Vandrovcova J, *et al.* Genome, transcriptome and proteome: the rise of omics data and their integration in biomedical sciences. *Brief Bioinform*. 2018;**19**:286–302. https://doi.org/10.1093/bib/bbw114.
5. Chakraborty S, Sharma G, Karmakar S, *et al.* Multi-OMICS approaches in cancer biology: new era in cancer therapy. *Biochim Biophys Acta Mol Basis Dis*. 2024;**1870**:167120. https://doi.org/10.1016/j.bbadis.2024.167120.
6. Huang C-Y, Huang W-K, Yeh K-Y, *et al.* Integrating comprehensive genomic profiling in the management of oncology patients: applications and challenges in Taiwan. *Biomed J*. 2025;**48**:100851. https://doi.org/10.1016/j.bj.2025.100851.
7. Bose A, Datta S, Mandal R, *et al.* Increased heterogeneity in expression of genes associated with cancer progression and drug resistance. *Transl Oncol*. 2024;**41**:101879. https://doi.org/10.1016/j.tranon.2024.101879.
8. Ferlier T, Coulouarn C. Regulation of gene expression in cancer—an overview. *Cells*. 2022;**11**:4058. https://doi.org/10.3390/cells11244058.
9. Hanahan D. Hallmarks of cancer: new dimensions. Cancer discov. 2022;**12**:31–46. https://doi.org/10.1158/2159-8290.CD-21-1059.
10. Li W, Ballard J, Zhao Y, *et al.* Knowledge-guided learning methods for integrative analysis of multi-omics data. *Comput Struct Biotechnol J*. 2024;**23**:1945–1950. https://doi.org/10.1016/j.csbj.2024.04.053.
11. Crick FHC. Central dogma of molecular biology. *Nature*. 1970;**227**:561–563. https://doi.org/10.1038/227561a0.
12. Pan Y, Lei X, Zhang Y. Association predictions of genomics, proteinomics, transcriptomics, microbiome, metabolomics, pathomics, radiomics, drug, symptoms, environment factor, and disease networks: a comprehensive approach. *Med Res Rev*. 2022;**42**:441–461. https://doi.org/10.1002/med.21847.
13. Panditrao G, Bhowmick R, Meena C, *et al.* Emerging landscape of molecular interaction networks: opportunities, challenges and prospects. *J Biosci*. 2022;**47**:24. https://doi.org/10.1007/s12038-022-00253-y.
14. Luo Y, Zhao C, Chen F. Multiomics research: principles and challenges in Integrated analysis. *BioDesign Res*. 2024;**6**:0059. https://doi.org/10.34133/bdr.0059.
15. Subramanian I, Verma S, Kumar S, *et al.* Multi-omics data integration, interpretation, and its application. *Bioinform Biol Insights*. 2020;**14**:117793221989905. https://doi.org/10.1177/1177932219899051.
16. Thapa K, Kinali M, Pei S, *et al.* Strategies to include prior knowledge in omics analysis with deep neural networks. *Patterns*. 2025;**6**:101203. https://doi.org/10.1016/j.patter.2025.101203.
17. Liu J, Cen X, Yi C, *et al.* Challenges in AI-driven biomedical multimodal data fusion and analysis. *Genomics Proteomics Bioinformatics*. 2025;**23**:qzaf011. https://doi.org/10.1093/gpbjnl/qzaf011.
18. Ballard JL, Wang Z, Li W, *et al.* Deep learning-based approaches for multi-omics data integration and analysis. *BioData Min*. 2024;**17**:38. https://doi.org/10.1186/s13040-024-00391-z.
19. Cai Z, Poulos RC, Liu J, *et al.* Machine learning for multi-omics data integration in cancer. *iScience*. 2022;**25**:103798. https://doi.org/10.1016/j.isci.2022.103798.
20. Yao X, Jiang X, Luo H, *et al.* MOCAT: multi-omics integration with auxiliary classifiers enhanced autoencoder. *BioData Min*. 2024;**17**:9. https://doi.org/10.1186/s13040-024-00360-6.

21. Zhao C, Liu A, Zhang X, *et al.* CLCLSA: cross-omics linked embedding with contrastive learning and self attention for integration with incomplete multi-omics data. *Comput Biol Med*. 2024;**170**:108058. https://doi.org/10.1016/j.compbiomed.2024.108058.
22. Lu Y, Peng R, Dong L, *et al.* Multiomics dynamic learning enables personalized diagnosis and prognosis for pancancer and cancer subtypes. *Brief Bioinform*. 2023;**24**:bbad378. https://doi.org/10.1093/bib/bbad378.
23. Valous NA, Popp F, Zörnig I, *et al.* Graph machine learning for integrated multi-omics analysis. *Br J Cancer*. 2024;**131**:205–211. https://doi.org/10.1038/s41416-024-02706-7.
24. Khoshraftar S, An A. A survey on graph representation learning methods. *ACM Trans Intell Syst Technol*. 2024;**15**:1–55. https://doi.org/10.1145/3633518.
25. Khemani B, Patil S, Kotecha K, *et al.* A review of graph neural networks: concepts, architectures, techniques, challenges, datasets, applications, and future directions. *J Big Data*. 2024;**11**:18. https://doi.org/10.1186/s40537-023-00876-4.
26. Kipf TN, Welling M. Semi-supervised classification with graph convolutional networks. *International Conference on Learning Representations (ICLR)*, 2017. https://openreview.net/forum?id=SJU4ayYgl. Accessed 28 October 2026.
27. Wang T, Shao W, Huang Z, *et al.* MOGONET integrates multi-omics data using graph convolutional networks allowing patient classification and biomarker identification. *Nat Commun*. 2021;**12**:3445. https://doi.org/10.1038/s41467-021-23774-w.
28. Li X, Ma J, Leng L, *et al.* MoGCN: a multi-omics integration method based on graph convolutional network for cancer subtype analysis. *Front Genet*. 2022;**13**:806842. https://doi.org/10.3389/fgene.2022.806842.
29. Xiao S, Lin H, Wang C, *et al.* Graph neural networks with multiple prior knowledge for Multi-omics data analysis. *IEEE J Biomed Health Inform*. 2023;**27**:4591–4600. https://doi.org/10.1109/JBHI.2023.3284794.
30. Alif MN, Zhang W. SynOmics: integrating multi-omics data through feature interaction networks. *Brief Bioinform*. 2025;**26**:bbaf595; https://doi.org/10.1093/bib/bbaf595.
31. Li B, Nabavi S. A multimodal graph neural network framework for cancer molecular subtype classification. *BMC Bioinf*. 2024;**25**:27; https://doi.org/10.1186/s12859-023-05622-4.
32. Veličković P, Cucurull G, Casanova A, *et al.* Graph attention networks. *International Conference on Learning Representations (ICLR)*, 2018. https://openreview.net/forum?id=rJXMpikCZ. Accessed 28 October 2026.
33. Kustatscher G, Collins T, Gingras AC, *et al.* Understudied proteins: opportunities and challenges for functional proteomics. *Nat Methods*. 2022;**19**:774–779. https://doi.org/10.1038/s41592-022-01454-x.
34. Dong L, Lu D, Chen R, *et al.* Proteogenomic characterization identifies clinically relevant subgroups of intrahepatic cholangiocarcinoma. *Cancer Cell*. 2022;**40**:70–87.e15. https://doi.org/10.1016/j.ccell.2021.12.006.
35. Mun D-G, Bhin J, Kim S, *et al.* Proteogenomic characterization of human early-onset gastric cancer. *Cancer Cell*. 2019;**35**:111–124.e10. https://doi.org/10.1016/j.ccell.2018.12.003.
36. Gao Q, Zhu H, Dong L, *et al.* Integrated proteogenomic characterization of HBV-related hepatocellular carcinoma. *Cell*. 2019;**179**:561–577.e22. https://doi.org/10.1016/j.cell.2019.08.052.
37. Veličković P, Fedus W, Hamilton WL, *et al.* Deep Graph Infomax. *International Conference on Learning Representations (ICLR)*, 2019. https://openreview.net/forum?id=rklz9iAcKQ. Accessed 28 October 2026.
38. Vaswani A, Shazeer N, Parmar N, *et al.* Attention is all you need. *Advances in Neural Information Processing Systems*, 2017;30. https://proceedings.neurips.cc/paper/2017/hash/3f5ee243547dee91fbd053c1c4a845aa-Abstract.html. Accessed 28 October 2026.
39. Arevalo J, Solorio T, Montes-y-Gómez M, *et al.* Gated multimodal networks. *Neural Comput Applic*. 2020;**32**:10209–10228. https://doi.org/10.1007/s00521-019-04559-1.
40. Chen W, Qiu H. MGDMCL: a multi-omics integration framework based on masked graph dynamic learning and multi-granularity feature contrastive learning for biomedical classification. *Comput Methods Programs Biomed*. 2025;**271**:109024. https://doi.org/10.1016/j.cmpb.2025.109024.
41. Wu H, Wu H, Xin X, *et al.* MOGANet: a multi-omics graph attention network for cancer diagnosis and biomarker identification. *Interdiscip Sci Comput Life Sci*. 2026; https://doi.org/10.1007/s12539-026-00828-5.
42. Shuken SR. An introduction to mass spectrometry-based proteomics. *J Proteome Res*. 2023;**22**:2151–2171. https://doi.org/10.1021/acs.jproteome.2c00838.
43. Oughtred R, Rust J, Chang C, *et al.* The BioGRID database: a comprehensive biomedical resource of curated protein, genetic, and chemical interactions. *Protein Sci*. 2021;**30**:187–200. https://doi.org/10.1002/pro.3978.
44. Szklarczyk D, Kirsch R, Koutrouli M, *et al.* The STRING database in 2023: protein–protein association networks and functional enrichment analyses for any sequenced genome of interest. *Nucleic Acids Res*. 2023;**51**:D638–D646. https://doi.org/10.1093/nar/gkac1000.
45. Breiman L. Random forests. *Mach Learn*. 2001;**45**:5–32. https://doi.org/10.1023/A:1010933404324.
46. Suykens JAK, Vandewalle J. Least squares support vector machine classifiers. *Neural Process Lett*. 1999;**9**:293–300. https://doi.org/10.1023/A:1018628609742.
47. Buckley J, James I. Linear regression with censored data. *Biometrika*. 1979;**66**:429–436. https://doi.org/10.1093/biomet/66.3.429.
48. Zhao S, Sun J, Yin Y, *et al.* MOAEAM: multi-omics data integration with autoencoder and attention mechanisms for cancer patient classification and biomarker identification. *IEEE J Biomed Health Inform*. 2026;**30**:3991–4001. https://doi.org/10.1109/JBHI.2025.3628490.
49. Wu Z, Pan S, Long G, *et al.* Beyond low-pass filtering: graph convolutional networks with automatic filtering. *IEEE Trans Knowl Data Eng*. 2023;**35**:6687–6697. https://doi.org/10.1109/TKDE.2022.3186016.
50. Li Q, Han Z, Wu X-M. Deeper insights into graph convolutional networks for semi-supervised learning. *Proc AAAI Conf Artif Intell*. 2018;**32**:3538–3545. https://doi.org/10.1609/aaai.v32i1.11604.

51. Wu Y, Hu X, Fan X, *et al.* Learning data-driven propagation mechanism for graph neural network. *Electronics*. 2023;**12**:46. https://doi.org/10.3390/electronics12010046.
52. Sun F-Y, Hoffmann J, Verma V, *et al.* InfoGraph: unsupervised and semi-supervised graph-level representation learning via mutual information maximization. *International Conference on Learning Representations (ICLR)*, 2020. https://openreview.net/forum?id=r1lfF2NYvH. Accessed 28 October 2026.
53. Hjelm RD, Fedorov A, Lavoie-Marchildon S, *et al.* Learning deep representations by mutual information estimation and maximization. *International Conference on Learning Representations (ICLR)*, 2019. https://openreview.net/forum?id=Bklr3j0cKX. Accessed 28 October 2026.
54. Hassani K, Khasahmadi AH. Contrastive multi-view representation learning on graphs. *Proceedings of the 37th International Conference on Machine Learning.* 2020;**119**:4116–4126. https://proceedings.mlr.press/v119/hassani20a.html. Accessed 28 October 2026.
55. You Y, Chen T, Sui Y, *et al.* Graph contrastive learning with augmentations. *Advances in Neural Information Processing Systems*, 2020;33. https://proceedings.neurips.cc/paper/2020/hash/3fe230348e9a12c13120749e3f9fa4cd-Abstract.html. Accessed 28 October 2026.
56. Zhang L, Dong X, Jia S, *et al.* Node2Vec-DGI-EL: a hierarchical graph representation learning model for ingredient–disease association prediction. *Bioinforma Adv*. 2026;**6**:vbaf216. https://doi.org/10.1093/bioadv/vbaf216.
57. Yan R, Islam MT, Xing L. Deep representation learning of protein–protein interaction networks for enhanced pattern discovery. *Sci Adv*. 2024;**10**:eadq4324. https://doi.org/10.1126/sciadv.adq4324.
58. Wang P, Wen X, Li H, *et al.* Deciphering driver regulators of cell fate decisions from single-cell transcriptomics data with CEFCON. *Nat Commun*. 2023;**14**:8459. https://doi.org/10.1038/s41467-023-44103-3.
59. Savage SR, Yi X, Lei JT, *et al.* Pan-cancer proteogenomics expands the landscape of therapeutic targets. *Cell*. 2024;**187**:4389–4407.e15. https://doi.org/10.1016/j.cell.2024.05.039.
60. Feng Y, Wang J, He R, *et al.* A retrieval-augmented knowledge mining method with deep thinking LLMs for biomedical research and clinical support. *GigaScience*. 2025;**14**:giaf109. https://doi.org/10.1093/gigascience/giaf109.
61. Feng Y, Zhou L, Ma C, *et al.* Knowledge graph-based thought: a knowledge graph–enhanced LLM framework for pan-cancer question answering. *GigaScience*. 2025;**14**:giae082. https://doi.org/10.1093/gigascience/giae082.
62. Dong Y, Zhou S, Xing L, *et al.* Deep learning methods may not outperform other machine learning methods on analyzing genomic studies. *Front Genet*. 2022;**13**:992070. https://doi.org/10.3389/fgene.2022.992070.
63. Sundararajan M, Taly A, Yan Q. Axiomatic attribution for deep networks. *Proceedings of the 34th International Conference on Machine Learning (PMLR).* 2017;**70**:3319–3328. https://proceedings.mlr.press/v70/sundararajan17a.html. Accessed 28 October 2026.
64. Liao Y, Savage SR, Dou Y, *et al.* A proteogenomics data-driven knowledge base of human cancer. *Cell Syst*. 2023;**14**:777–787.e5. https://doi.org/10.1016/j.cels.2023.07.007.
65. Ji Y, Dutta P, Davuluri R. Deep multi-omics integration by learning correlation-maximizing representation identifies prognostically stratified cancer subtypes. *Bioinforma Adv*. 2023;**3**:vbad075. https://doi.org/10.1093/bioadv/vbad075.
66. Pastrello C, Kotlyar M, Jurisica I. Informed use of protein–protein interaction data: a focus on the integrated interactions database (IID). *Methods Mol Biol*. 2020; **2074**:125–134. https://doi.org/10.1007/978-1-4939-9873-9_10.
67. Gong J, Shao D, Xu K, *et al.* RISE: a database of RNA interactome from sequencing experiments. *Nucleic Acids Res*. 2018;**46**:D194–D201. https://doi.org/10.1093/nar/gkx864.
68. Zheng Y, Luo H, Teng X, *et al.* NPInter v5.0: ncRNA interaction database in a new era. *Nucleic Acids Res*. 2023;**51**:D232–D239. https://doi.org/10.1093/nar/gkac1002.
69. Kang J, Tang Q, He J, *et al.* RNAInter v4.0: RNA interactome repository with redefined confidence scoring system and improved accessibility. *Nucleic Acids Res*. 2022;**50**:D326–D332. https://doi.org/10.1093/nar/gkab997.
70. Chang L, Zhou G, Soufan O, *et al.* miRNet 2.0: network-based visual analytics for miRNA functional analysis and systems biology. *Nucleic Acids Res*. 2020;**48**:W244–W251. https://doi.org/10.1093/nar/gkaa467.
71. Lin T-Y, Goyal P, Girshick R, *et al.* Focal loss for dense object detection. *IEEE Trans Pattern Anal Mach Intell*. 2020;**42**:318–327. https://doi.org/10.1109/TPAMI.2018.2858826.
72. Akiba T, Sano S, Yanase T, *et al.* Optuna: a next-generation hyperparameter optimization framework. *Proc 25th ACM SIGKDD Int Conf Knowl Discov Data Min*. 2019;2623–2631. https://doi.org/10.1145/3292500.3330701. Accessed 28 October 2026.

Received: 28 May 2026. **Revised:** 31 August 2026. **Accepted:** 16 October 2026
© The Author(s) 2026. Published by Oxford University Press on behalf of GigaScience. This is an Open Access article distributed under the terms of the Creative Commons Attribution License (https://creativecommons.org/licenses/by/4.0/), which permits unrestricted reuse, distribution, and reproduction in any medium, provided the original work is properly cited.